Intracellular Cl^- as a signaling ion that potently regulates $Na^+/HCO3^-$ transporters

Nikolay Shcheynikov[a,1], Aran Son[a,1], Jeong Hee Hong[a,b,1], Osamu Yamazaki[a], Ehud Ohana[c], Ira Kurtz[d,e], Dong Min Shin[f,2], and Shmuel Muallem[a,2]

[a]Epithelial Signaling and Transport Section, Molecular Physiology and Therapeutics Branch, National Institute of Dental and Craniofacial Research, NIH, Bethesda, MD 20892; [b]Department of Physiology, Graduate School of Medicine, Gachon University, Yeonsu-gu, Incheon, 406-799, South Korea; [c]Department of Clinical Biochemistry and Pharmacology, the Faculty of Health Sciences, Ben Gurion University of the Negev, 8410501 Bear Sheva, Israel; [d]Division of Nephrology, Department of Medicine, and [e]Brain Research Institute, University of California, Los Angeles, CA 90095; and [f]Department of Oral Biology, BK 21 PLUS Project, Yonsei University College of Dentistry, Seoul 120-752, Korea

Edited* by Melanie H. Cobb, University of Texas Southwestern Medical Center, Dallas, TX, and approved December 8, 2014 (received for review August 13, 2014)

Cl^- is a major anion in mammalian cells involved in transport processes that determines the intracellular activity of many ions and plasma membrane potential. Surprisingly, a role of intracellular Cl^- (Cl^-_{in}) as a signaling ion has not been previously evaluated. Here we report that Cl^-_{in} functions as a regulator of cellular Na^+ and HCO_3^- concentrations and transepithelial transport through modulating the activity of several electrogenic Na^+-HCO_3^- transporters. We describe the molecular mechanism(s) of this regulation by physiological Cl^-_{in} concentrations highlighting the role of GXXXP motifs in Cl^- sensing. Regulation of the ubiquitous Na^+-$HCO3^-$ cotransport (NBC)e1-B is mediated by two GXXXP-containing sites; regulation of NBCe2-C is dependent on a single GXXXP motif; and regulation of NBCe1-A depends on a cryptic GXXXP motif. In the basal state NBCe1-B is inhibited by high Cl^-_{in} interacting at a low affinity GXXXP-containing site. IP_3 receptor binding protein released with IP_3 (IRBIT) activation of NBCe1-B unmasks a second high affinity Cl^-_{in} interacting GXXXP-dependent site. By contrast, NBCe2-C, which does not interact with IRBIT, has a single high affinity N-terminal GXXP-containing Cl^-_{in} interacting site. NBCe1-A is unaffected by Cl^-_{in} between 5 and 140 mM. However, deletion of NBCe1-A residues 29–41 unmasks a cryptic GXXXP-containing site homologous with the NBCe1-B low affinity site that is involved in inhibition of NBCe1-A by Cl^-_{in}. These findings reveal a cellular Cl^-_{in} sensing mechanism that plays an important role in the regulation of Na^+ and HCO_3^- transport, with critical implications for the role of Cl^- in cellular ion homeostasis and epithelial fluid and electrolyte secretion.

intracellular Cl^- | signaling ion | transporters

Cl^- and HCO_3^- are the two major intracellular anions in mammalian cells. Specific transporters, channels, and the membrane potential tightly regulate their extracellular and intracellular concentrations. In turn, Cl^- and HCO_3^- regulate the concentration of other ions, including Na^+, K^+, and SO_4^{2-}, either directly or indirectly. Known ubiquitous Cl^-- and HCO_3^--coupled transporters include the NaCl cotransporters NCCs, the KCl cotransporters KCCs, the $Na^+/K^+/2Cl^-$ cotransporter NKCC1 (1), the SLC26 Cl^-/HCO_3^- exchangers and channels (2, 3), and members of the SLC4 exchangers and cotransporters family (4). The intracellular Cl^- (Cl^-_{in}) concentration is also regulated by the ClCs (5) and Anoctamines Cl^- channels (6). Cl^- plays a role in a wide variety of cellular transport functions, including regulation of the membrane potential (6), cell volume (2), systemic and cellular acid–base balance (4), and transepithelial fluid and electrolyte secretion (7). In addition, Cl^- was reported to regulate transient receptor potential (TRP) channels (8), receptors assembly and function (9–11), activation of Neutrophil β2 Integrins (12), and the cell cycle (13).

Like Cl^-, HCO_3^- also has many important physiological roles, being the principal biological pH buffer (7) and an activator of the soluble adenylyl cyclase (14). In epithelia, HCO_3^- has a key role in tissue/cell viability. Among other fundamental roles, HCO_3^- drives Cl^- absorption and fluid secretion, stimulates mucin secretion, and controls solubilization of secreted macromolecules (7). Epithelial HCO_3^- secretion is fueled by the cellular Na^+ gradient, which provides the driving force for HCO_3^- entry across the basolateral membrane mediated by the Na^+-HCO_3^- cotransport NBCe1-B. HCO_3^- then exits the luminal membrane by the coordinated and coupled functions of the Cl^- channel cystic fibrosis transmembrane conductance regulator (CFTR) and the electrogenic Cl^-/HCO_3^- exchanger slc26a6 (3, 7, 15). In the kidney, NBCe1-A mediates basolateral HCO_3^- extrusion (16, 17). In secretory ducts the basolateral NBCe1-B–mediated HCO_3^- influx is coupled to apical HCO_3^- secretion and Cl^- absorption via CFTR and slc26a6 (7). Cl^-_{in} is reduced along the ducts as luminal Cl^- is reduced and luminal HCO_3^- is increased (18, 19).

Members of the SLC4 superfamily of HCO_3^- cotransporters are key transporters involved in cellular HCO_3^- and Cl^- homeostasis (4, 7). The family consists of several subfamilies, including the electrogenic NBCe1 and NBCe2, electroneutral NBCn1 and NBCn2, Cl^--coupled anion exchangers AEs, and the Na^+-dependent Cl^-/HCO_3^- exchanger NDCBE (4). In a wide variety of tissues, NBCe1-B mediates the electrogenic transport of $1Na^+$ and $2HCO_3^-$ ions (likely Na^+-CO_3^{2-}) (4, 17) and

Significance

Cl^- is the major cellular anion that controls the intracellular activity of many ions, the membrane potential, and transepithelial fluid and electrolyte secretion. How cells sense intracellular Cl^- (Cl^-_{in}) to coordinate all Cl^--dependent activities is not known. We report a molecular mechanism for Cl^-_{in} sensing that involves interaction of Cl^- with GXXXP-containing sites and show how these sites are used to regulate the activity of several Na^+-HCO_3^- cotransporters. Although these transporters do not transport Cl^-, they sense Cl^-_{in} in a manner specific for each transporter that is suitable for the transporter physiological activity. Our data has fundamental implications for the role of Cl^- in cellular ion homeostasis and fluid and electrolyte secretion.

Author contributions: D.M.S. and S.M. designed research; N.S., A.S., J.H.H., and O.Y. performed research; I.K. contributed new reagents/analytic tools; N.S., A.S., J.H.H., O.Y., E.O., D.M.S., and S.M. analyzed data; N.S., E.O., I.K., D.M.S., and S.M. wrote the paper; and E.O. did modeling.

The authors declare no conflict of interest.

*This Direct Submission article had a prearranged editor.

[1]N.S., A.S., and J.H.H. contributed equally to this work.

[2]To whom correspondence may be addressed. Email: dmshin@yuhs.ac or Shmuel.Muallem@nih.gov.

This article contains supporting information online at www.pnas.org/lookup/suppl/doi:10.1073/pnas.1415673112/-/DCSupplemental.

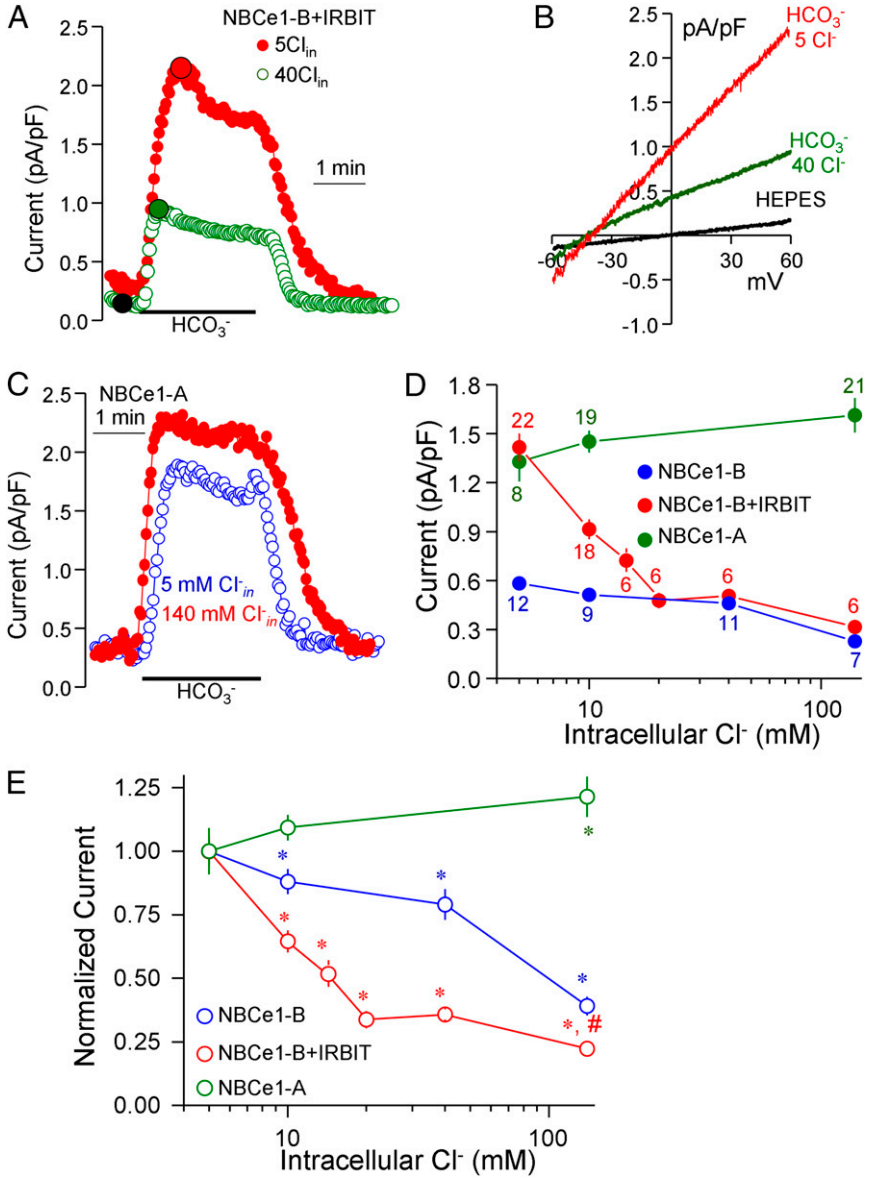

Fig. 1. Effect of Cl^-_{in} on the activity of NBCe1-B and NBCe1-A. (*A*) Example traces of current measured in HeLa cells expressing NBCe1-B and IRBIT and in pipette solutions containing 5 or 40 mM Cl^-; (*B*) I/V plots at the times indicated by the black circles in each trace. All I/V plots show the raw current under each condition. (*C*) Example traces of current recorded in HeLa cells expressing NBCe1-A with pipette solution containing 5 or 140 mM Cl^-. (*D* and *E*) Cl^-_{in}-dependence of the current density in pA/pF (*D*) and normalization to the current measured at 5 mM Cl^-_{in} at each of the conditions (*E*) in cells expressing NBCe1-B alone (blue), NBCe1-B+IRBIT (red), or NBCe1-A (green). The numbers next to the traces indicate the number of experiments. Results are given as mean ± SEM. In *E*: $^*P < 0.01$ or better relative to NBCe1-B activity at 5 mM Cl^-_{in}; $^{\#}P < 0.05$ relative to NBCe1-B in the absence of IRBIT with pipette solution containing 140 mM Cl^-_{in}.

functions as the main epithelial HCO_3^- entry mechanism in the basolateral membrane of polarized cells (7). Cell-specific electrogenic NBC transporters include NBCe1-A, which is expressed in the basolateral membrane of the renal proximal tubule (4, 17), and NBCe2-C, which is found in the choroid plexus (20). IRBIT, which regulates NBCe1-B (21–23) and NBCn1-A (24), binds to the IP_3 binding domain of the IP_3 receptors (IP_3Rs) (25). IRBIT is released from the IP_3Rs upon an increase in cellular IP_3 (26), becoming available for regulation of NBCe1-B (21–23), NBCn1-A (24), CFTR (22, 23), and slc26a6 (27), thereby coordinating the activation of these transporters and epithelial fluid and HCO_3^- secretion (27).

Cl^-_{in} has not been previously considered as a signaling ion. Rather, Cl^- has heretofore mainly been viewed as an ion that is transported by various channels, coupled to Na^+, K^+, or HCO_3^- transport, and that plays a role regulating the plasma membrane potential (1, 7). Importantly, several studies have provided clues that Cl^-_{in} may have regulatory and perhaps signaling functions. High Cl^-_{in} was reported to inhibit the activity of the epithelial Na^+ channel ENaC (28), the permeability of CFTR to HCO_3^- (29), TRPM7 activity (8), and perhaps the activity of the Na^+/H^+ exchanger NHE1 (30). Muscarinic stimulation of salivary gland acinar cells resulted in reduction in Cl^-_{in} that is required for Na^+ influx by the Na^+/H^+ exchanger and the $Na^+/K^+/2Cl^-$ cotransporter (31).

In the present study we asked whether Cl^-_{in} functions as a signaling ion that modulates cellular Na^+ and HCO_3^- concentrations through regulation of electrogenic NBC transporters.

Our data indicate that Cl^-_{in} regulates the function of NBCe1-B, NBCe2-C, and NBCe1-A via a cryptic Cl^- sites. In the basal state NBCe1-B is inhibited by Cl^-_{in} interacting with a low affinity Cl^- site, whereas NBCe1-A is resistant to Cl^-_{in}. By contrast, IRBIT-activated NBCe1-B is inhibited by low and high concentrations of Cl^-_{in} due to interaction with high and low affinity Cl^-_{in} motifs that depend on GXXXP motifs. Mutation of the G and P or of His in GXHXP in the autoinhibitory domain of NBCe1-B eliminated inhibition by low Cl^-_{in}, whereas sparing inhibition of NBCe1-B by high Cl^-_{in}. Mutation of a second GXXXP motif was required to eliminate inhibition by low affinity Cl^-_{in} site. NBCe2-C is inhibited by a single high affinity GXXXP motif-dependent Cl^-_{in} interacting site. Remarkably, deletion of the first 48 residues of NBCe1-A or of residues 29–41 uncovered inhibition of NBCe1-A by Cl^-_{in} that was mediated by a GXXXP motif-dependent site homologous with the second GXXXP motif of NBCe1-B. These findings reveal a Cl^-_{in} sensing mechanism that modulates the activity of NBCe1-B, NBCe2-C, and NBCe1-A. In transporting epithelia, such as the pancreatic and salivary ducts and the choroid plexus, we predict that a reduction in Cl^-_{in} will dramatically increase transepithelial HCO_3^- transport and fluid secretion.

Results

Cl^-_{in} Inhibits NBCe1-B but Not NBCe1-A. The activity of the electrogenic NBCe1-A, NBCe1-B, and NBCe2-C were monitored by measuring the Na^+-dependent HCO_3^- current. In previous studies we showed that NBCe1-A and NBCe1-B currents can be accurately measured by expressing the transporters in HeLa cells and measuring whole-cell currents (24). The modulation of Cl^-_{in} was achieved by varying the Cl^- concentration in the pipette solution. Fig. 1*A* shows example current traces, and Fig. 1*B* shows the current/voltage (I/V) relationships measured in cells expressing NBCe1-B in the presence of IRBIT, and in the presence of 5 or 40 mM Cl^-_{in}. The I/Vs show the raw current under each conditions. To calculate the HCO_3^--activated current density, the leak current measured in Hepes-buffered medium before addition of HCO_3^- was subtracted from the total current in the presence of HCO_3^- and normalized to the cell capacitance. Current densities are shown in Fig. 1*D*, and Fig. 1*E* shows the current normalized to that measured at 5 mM Cl^-_{in} under each condition. When NBCe1-B was expressed alone, raising Cl^-_{in} between 5 and 40 mM only modestly inhibited transport activity by approximately 20%, whereas raising Cl^-_{in} to a nonphysiological concentration of 140 mM inhibited NBCe1-B activity by approximately 60%, with an EC_{50} of approximately 56 ± 4 mM. On the other hand, when NBCe1-B was activated by IRBIT to prevent autoinhibition (21–23), raising Cl^-_{in} from 5 to 20 mM strongly inhibited NBCe1-B activity by approximately 65%, with an apparent K_i of 10.2 ± 0.3 mM. Further increasing Cl^-_{in} to 140 mM inhibited the activity by an additional 15%. The inhibition by Cl^-_{in} did not seem to change the reversal potential of the HCO_3^--activated currents, suggesting that Cl^- does not affect NBCe1-B stoichiometry. Finally, similar experiments with NBCe1-A showed that rising Cl^-_{in} up to 140 mM actually increased the activity of NBCe1-A by ~20% (Fig. 1 *C*–*E*).

To determine the specificity of the inhibition, we tested the effect of extracellular Cl^- (Cl^-_{out}) and of other intracellular halides. Fig. S1*A* shows that removal of Cl^-_{out} minimally inhibited the current, as was observed on the leak current. Correction for the effect of Cl^-_{out} on the leak current shows that Cl^-_{out} had no statistical effect on NBCe1-B activity (Fig. S1*B*). Fig. S2 *C* and *D* show that the effect of Cl^-_{in} is highly specific in that raising Cl^-_{in} from 5 to 10 mM inhibited NBCe1-B by approximately 40%, whereas addition of 5 mM intracellular Br^-, I^-, or NO_3^- had no effect.

Regulation by Cl^-_{in} Is Mediated by NBCe1-B GXXXP Motifs. A GXXXP motif was identified as an essential part of a Cl^- interacting site in the ClC Cl^- transporters (32, 33). Mutations within this motif altered Cl^- transport and coupling in ClCs (34, 35). Recently, we reported that regulation of slc26a2 by extracellular Cl^- is altered by mutations in slc26a2 GXXXP motif (36). NBCe1-B has three GXXXP motifs in the N terminus (Fig. S2), with the first motif in the autoinhibitory domain (AID) that is present in many NBCs, but not in NBCe1-A (Fig. S2*A*). The predicted localization of the GXXXP motifs in the N terminus of NBCe1-B and their potential contacts are modeled in Fig. S3. Several regulatory factors, including inhibition by the WNK/SPAK pathway and activation by the IRBIT/PP1 pathway (22, 24) and by $PI(4,5)P_2$ (24), converge on the AID, and thus we asked whether regulation by Cl^-_{in} requires the AID GXXXP motif. Because the high affinity inhibition by Cl^-_{in} is seen only after activation of NBCe1-B by IRBIT, we determined how mutations of residues in the AID GXXXP motif (Fig. 2*A*) affect the activity of NBCe1-B and regulation by IRBIT. Unexpectedly, Fig. 2*B* shows that mutating even a single residue in the GXXXP motif, the His to either Ala or to the reverse charge Asp, resulted in full activation of NBCe1-B and no further activation by IRBIT. Fig. 2*C* shows that mutation of the His and of the Gly and Pro in the GXXXP motif had no effect on IRBIT binding, indicating that the IRBIT binding domain [NBCe1-B-(40-62) (24)] is intact in these mutants. Rather, it is possible that the mutations caused a conformational change in the AID that prevented its interaction with another N terminus domain. Additional mutants were tested for the effect of Cl^-_{in} are NBCe1-B(Δ40-62) and NBCe1-B(Δ1-95). These mutants were used because they retain full activity (Fig. 2*B* and refs. 24 and 37), whereas NBCe1-B(Δ1-95) lacks the first GXXXP motif and NBCe1-B(Δ40-62) lacks IRBIT binding (Fig. 2*C*).

Fig. 3*A* shows that all mutations in the ^{32}GXXXP^{36} motif shifted the concentration dependence for inhibition by Cl^-_{in} to the right, resulting in an apparent K_i of 29.3 ± 2.6 mM, and that the inhibition was not affected further by coexpression of ^{32}GP^{36}/AA (and ^{34}H/A) with IRBIT. However, the activity of the mutants was still strongly inhibited at Cl^-_{in} above 20 mM. This may represent Cl^- binding to a site containing one of the other GXXXP motifs. To test these possibilities, the effect of mutating the other GXXXP motifs was tested. Mutation of the third ^{383}GXXXP^{387} motif of NBCe1-B and of the second ^{339}GXXXP^{343} motif of NBCe1-A, which are predicted to be at the boundary between the cytoplasmic N terminus and the transmembrane domains (Fig. S3), resulted in retention of the proteins in the ER, and thus the role of these motifs in inhibition by Cl^-_{in} could not be tested.

Mutating the second ^{195}GXXXP^{199} motif slightly reduced, but did not prevent, interaction of NBCe1-B with IRBIT (Fig. 2*D*). Nevertheless, the ^{195}GP^{199}/AA mutation resulted in full activation of the transporter in the absence of IRBIT, as evident from a lack of further activation by IRBIT (Fig. 3*B*). The ^{195}GP^{199}/AA mutation reduced the affinity for inhibition by Cl^-_{in} to a similar degree as the ^{32}GP^{36}/AA mutant. Importantly, NBCe1-B(^{32}GP^{36}/AA;^{195}GP^{199}/AA) with the first and second GXXXP motifs mutated was no longer inhibited by Cl^-_{in}. In addition, IRBIT interaction with the ^{195}GP^{199}/AA mutant also resulted in complete elimination of the inhibition by Cl^-_{in}. The latter would suggest that binding of IRBIT to NBCe1-B(^{195}GP^{199}/AA) induces a long range conformational change at the ^{32}GP^{36} region. To further probe the role of the two GXXXP motifs we measured the activity of NBCe1-B(Δ40-62) and NBCe1-B(Δ1-95) because these constructs retain full activity (ref. 37 and Fig. 2*A*) and NBCe1-B (Δ1-95) is missing the entire AID, including the ^{32}GXXXP^{36} motif. Fig. 3*D* shows that the two constructs lost inhibition by low Cl^-_{in} but retained inhibition by high Cl^-_{in} between 40 and 140 mM. As expected, mutation of the ^{195}GP^{199}/AA motif in NBCe1-B(Δ1-95) eliminated inhibition by Cl^-_{in}.

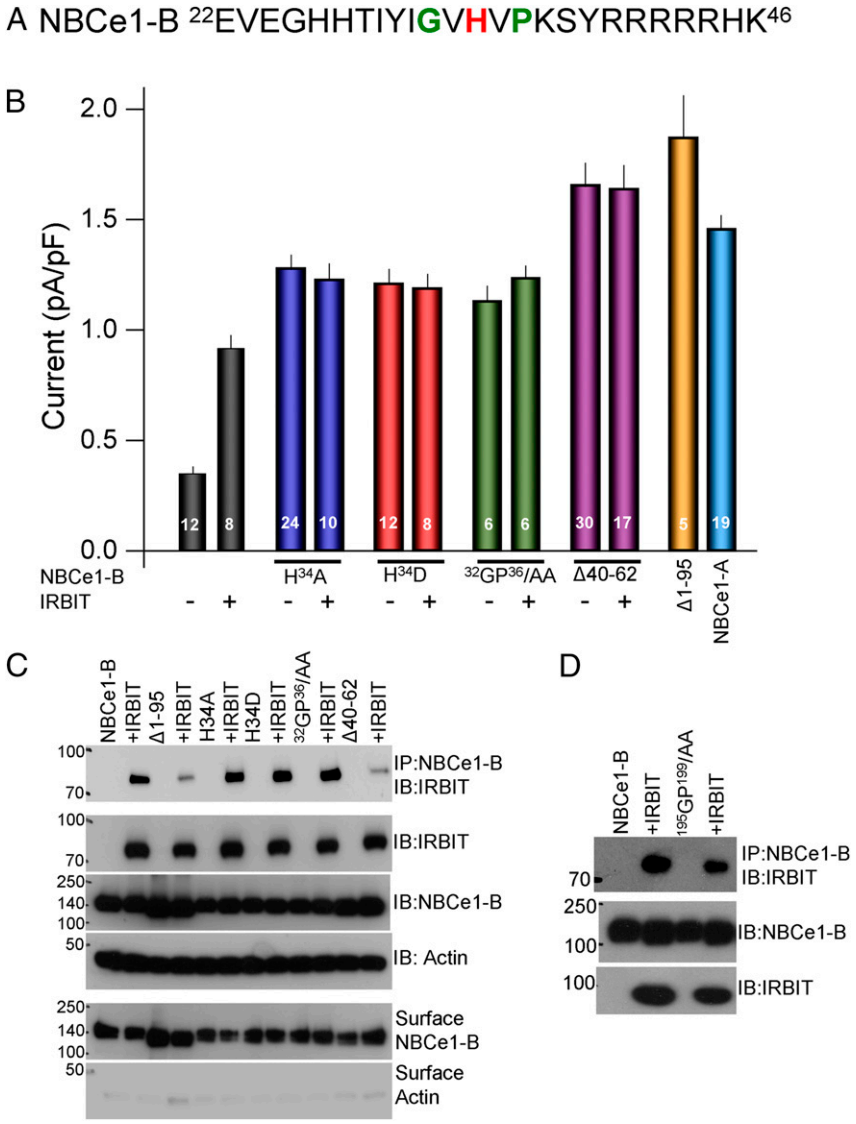

Fig. 2. Effect of NBCe1-B GXXXP motifs, NBCe1-B(Δ1-95), NBCe1-B(Δ40-62), and NBCe1-B(^{195}GP^{199}/AA) on NBCe1-B activity and interaction with IRBIT. (*A*) N-terminal sequence of NBCe1-B with the G, P, and H in the GXXXP motif that were mutated to A. (*B*) Summary of the current density in pA/pF of the indicated NBCe1-B mutants and in the presence and absence of IRBIT, as indicated. The last column shows the activity of NBCe1-A for comparison. The numbers in the columns are the number of experiments in each condition. Note that all NBCe1-B mutations eliminated activation of NBCe1-B by IRBIT. (*C*) Effect of the indicated NBCe1-B mutants on NBCe1-B surface expression and its interaction with IRBIT. Note that although the GXXXP motif mutations eliminated activation by IRBIT, they had no effect on IRBIT binding to NBCe1-B or NBCe1-B surface expression. (*D*) Mutation of the second NBCe1-B GXXXP motif (^{195}GP^{199}/AA) only slightly reduced interaction of NBCe1-B with IRBIT. The experiments in *C* and *D* are representative of three similar experiments.

The results in Figs. 1–3 suggest that the two NBCe1-B GXXXP motifs participate in sensing and regulation by Cl^-_{in}. The ^{32}GXXXP^{36} motif in the AID is cryptic and does not respond to Cl^-_{in} before its exposure by IRBIT. The second ^{195}GXXXP^{199} motif site mediates inhibition by high Cl^-_{in}. This is concluded from the data showing that NBCe1-B(^{32}GP^{36}/AA;^{195}GP^{199}/AA) activity in not inhibited by Cl^-_{in} and that NBCe1-B(Δ1-95) has low apparent affinity for Cl^-_{in} that is eliminated by the ^{195}GP^{199}/AA mutation.

A Cryptic Cl^-_{in}-Dependent Inhibitory Site in NBCe1-A. NBCe1-B(Δ1-95) retains inhibition by high Cl^-_{in}, and the sequence of NBCe1-B(96-1079) is identical to NBCe1-A(41-1024); yet NBCe1-A is resistant to inhibition by Cl^-_{in}. This suggests that NBCe1-A(1-41) may offer protection of NBCe1-A from inhibition by Cl^-_{in} and prompted us to test whether NBCe1-A is also regulated by a cryptic Cl^-_{in}-sensing site. Such regulation might be mediated by the conserved ^{150}GXXXP^{154} motif in NBCe1-A (Figs. S2 and S3). The experiments depicted in Fig. 4 attempted to test this hypothesis. Because no activator similar to IRBIT is known for NBCe1-A, we took the approach of systematic deletion of portions of NBCe1-A N terminus and tested for inhibition by 140 mM Cl^-_{in}. Previous studies reported that deletion of NBCe1-A (1-43) resulted in 50–70% inhibition of NBCe1-A activity when expressed in *Xenopus* oocytes, even in the presence of only 2 mM Cl^- (38). Therefore, in preliminary experiments we compared the activity of wild-type NBCe1-A and the truncation mutants examined in Fig. 4 in the presence of 5 mM Cl^-_{in}. Interestingly, the truncation had no effect on NBCe1-A activity when expressed in HeLa cells. This is shown for Δ13-NBCe1-A with deletion of residues 29–42. The reason for the different findings is not known at present, although it is possible that NBCs may behave differently in *Xenopus* oocytes and mammalian cells.

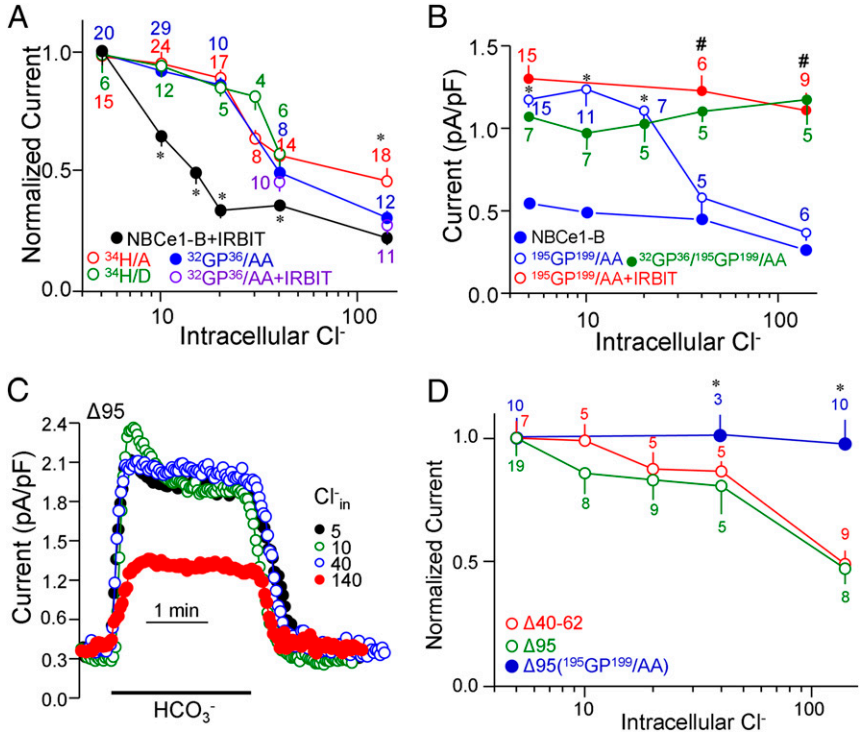

Fig. 3. Mutations of NBCe1-B GXXXP motifs alter inhibition by Cl^-_{in}. (*A*) Effect of the indicated first GXXXP motif mutants on inhibition of NBCe1-B by Cl^-_{in}. The results of NBCe1-B+IRBIT are reproduced from Fig. 1*E*. The numbers next to the symbols indicate the number of experiments with the corresponding currents. Note that although IRBIT binds to NBCe1-B(^{32}GP^{38}/AA), it had no further effect on the inhibition by Cl^-_{in}. *$P < 0.01$ relative to NBCe1-B+IRBIT for all conditions, except for 140 mM, where it is only for the NBCe1-B(^{34}H/A) mutant. (*B*) Effect of the NBCe1-B(^{195}GP^{199}/AA) mutant alone and of the double mutant NBCe1-B(^{32}GP^{38}/AA;^{195}GP^{199}/AA) on inhibition of NBCe1-B by Cl^-_{in}. The results of NBCe1-B are reproduced from Fig. 1*D*. The numbers next to the symbols indicate the number of experiments with the corresponding currents. Note that NBCe1-B(^{32}GP^{38}/AA;^{195}GP^{199}/AA) is not inhibited by Cl^-_{in} and that IRBIT eliminated inhibition of NBCe1-B(^{195}GP^{199}/AA) by Cl^-_{in}. *$P < 0.01$ relative to NBCe1-B; #$P < 0.001$ relative to NBCe1-B(^{195}GP^{199}/AA). (*C*) Example traces and (*D*) mean ± SEM of the current recorded with the indicated NBCe1-B mutants. Note that the ^{195}GP^{199}/AA mutation eliminated the residual low affinity inhibition of NBCe1-B(Δ1-95) by Cl^-_{in}. *$P < 0.05$ or better relative to NBCe1-B(Δ1-95).

The effect of the various NBCe1-A N-terminal truncations on inhibition by Cl^-_{in} is presented in Fig. 4*A*, which shows that deletion of the first 48 residues induced a ∼35% inhibition of NBCe1-A activity by 140 mM Cl^-_{in}. The NBCe1-A sequence required to observe the full inhibition by Cl^-_{in} was determined by the deletions depicted in Fig. 4*A*. Most deletions had no effect, but deletion of the 13 residues 29–42 to obtain Δ13-NBCe1-A resulted in the inhibition of NBCe1-A by Cl^-_{in} in the concentration range of 20–140 mM (Fig. 4*B*). Finally, the ^{150}GP^{154}/AA mutation in Δ13-NBCe1-A eliminated the inhibition by Cl^-_{in} (Fig. 4*B*). These findings indicate that NBCe1-A has a cryptic Cl^-_{in} interacting site. The data provide further evidence for the role this GXXXP motif in the inhibition by Cl^-_{in}.

The GXXXP Motif-Containing Site Mediates Regulation of NBCe2-C by Cl^-_{in}. Fig. S2*A* shows that the first GXXXP motif is present in most NBCs. To determine whether the first GXXXP motif is required for regulation by Cl^-_{in} in other NBCs, we evaluated its role in NBCe2-C, which was selected because it is an electrogenic Na^+-HCO_3^- cotransporter (39, 40), and thus the current mediated by NBCe2-C can be recorded while altering Cl^-_{in} in the patch pipette. First, we determined the effect of IRBIT on NBCe2-C. Fig. 5*A* shows that the positively charged arginine cluster required for regulation of the NBCs by IRBIT and $PI(4,5)P_2$ (24) (highlighted in red) is absent in NBCe2-C. The lack of activation of NBCe2-C by IRBIT is shown in Fig. 5*B*, further supporting the involvement of the arginine cluster in the regulation of other NBCs by IRBIT.

Fig. 5*C* shows examples of current density and the I/V curves mediated by NBCe2-C in the presence of 5 and 140 mM Cl^-_{in}. Cl^-_{in} strongly inhibited NBCe2-C activity, again without changing the reversal potential, and thus the stoichiometry of the transport process. The plot in Fig. 5*E* shows that Cl^-_{in} inhibited NBCe2-C by approximately 72%, with an apparent K_m of approximately 22.6 ± 3.2 mM. Notably, Fig. 5*D* (representative traces) and Fig. 5*E* show that the ^{34}GP^{38}/AA mutation virtually eliminated the inhibition by up to 140 mM Cl^-_{in}. Hence, it seems that the GXXXP motif is required for regulation of NBC transporters by Cl^-_{in}, which may be a property of other SLC4 family members possessing the GXXXP motif.

Discussion

Cl^- is a major cellular anion and participates in numerous cellular functions that contribute to ion and fluid homeostasis. Cl^-_{in} varies between 5 and 60 mM, depending on the cell type, and is determined by the activity of several ion/substrate transporters and ion channels. For example, in different neurons Cl^-_{in} is between 5 and 30 mM (41, 42), whereas in epithelia it is between 10 and 60 mM (19, 43, 44). Furthermore, Cl^-_{in} is not constant and can vary widely in specific cell types. Specifically, in secretory ducts the resting Cl^-_{in} is ∼35 mM and decreases to 4 mM toward the latter phase of Cl^- absorption and HCO_3^- secretion (7, 19).

The significance of changes in Cl^-_{in} has historically focused on the effect on plasma membrane Cl^- gradients and transepithelial Cl^- transport. The present study has uncovered a previously unidentified function of Cl^-_{in} as a signaling ion that regulates the activity of other transporters, including transporters that do not

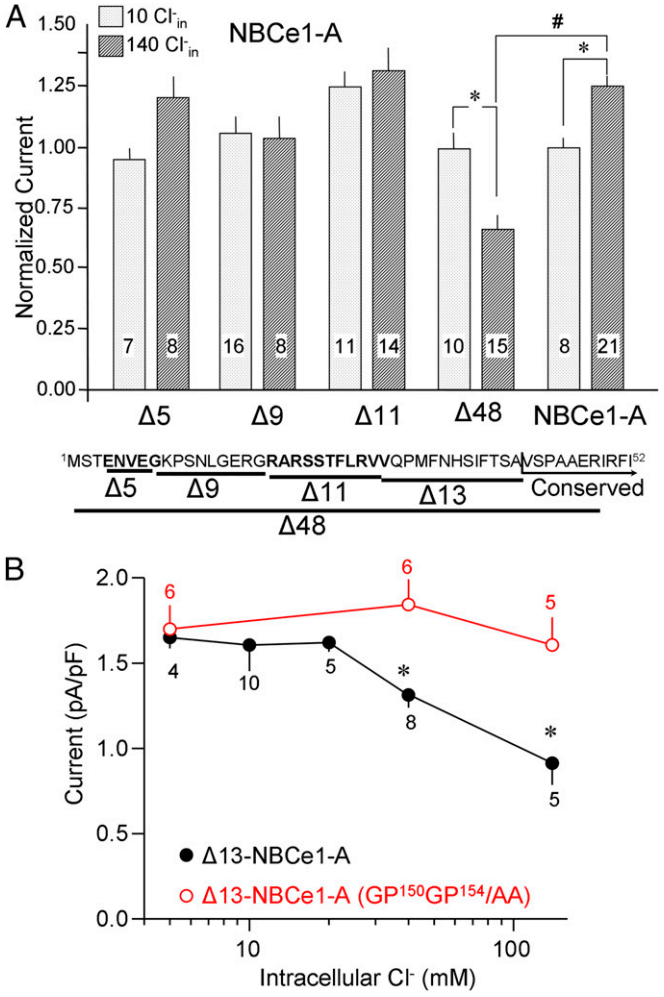

Fig. 4. A cryptic GXXXP motif mediates inhibition of NBCe1-A by Cl^-_{in}. (*A*) Comparison of the activity of NBCe1-A in the presence of 5 (dotted columns) or 140 (stripped columns) mM Cl^-_{in} of the indicated truncations in the N terminus, shown under the columns. The results are given as mean ± SEM of the number of experiments indicated in the columns. $^*P < 0.01$, $^\#P < 0.05$ relative to 140 mM Cl^-_{in} of the same mutant. (*B*) Effect of Cl^-_{in} on the activity of Δ13-NBCe1-A (black) and Δ13-NBCe1-A(^{150}GP^{154}/AA) (red). Results are given as mean ± SEM of the number of experiments indicated next to the symbols. $^*P < 0.01$ relative to Δ13-NBCe1-A.

transport Cl^-, such as the NBCs. The regulation seems to be mediated by sites containing GXXXP motifs, which have been associated with Cl^- sensing and transport in other transporters (32–36). In the ClC channels, residues in the GXXXP motifs from several regions are brought together to form the Cl^- binding sites (32). Altogether seven residues are involved in Cl^- binding. The conducting pore E148 is found in a GXXXP motif but does not participate in Cl^- binding. The other six residues that form polar and hydrophobic interactions generate an electrostatically favorable environment for anion binding (32). Hence, the environment generated by interactions of the GXXXP motif form the pocket in which several residues coordinate Cl^- binding. Indeed, translocation of the first NBCe1-B GXXXP motif GVHVP to another position in the N terminus or to the end of the C terminus failed to restore inhibition by Cl^-_{in}. Contribution of residues to the GXXXP motifs to form the Cl^- pocket makes it virtually impossible to predict the residues that cooperate with the NBCs GXXXP motifs to form the Cl^- binding sites without the actual structure. Nevertheless, potential interactions that the two GXXXP motifs in the NBCe1-B model form to coordinate Cl^- binding are shown in Fig. S3. The significance of these potential interactions awaits availability of the NBCe1-B structure.

Regulation by Cl^-_{in} differs in complexity depending on the NBC transporter involved. Regulation of NBCe2-C seems to be mediated mostly by the exposed first GXXXP motif. Inhibition by Cl^-_{in} did not require exposure of a cryptic site, and mutation of the first NBCe2-C GXXXP motif nearly eliminated inhibition by Cl^-_{in}. The simple regulation of NBCe2-C may reflect the lack of activation of this transporter by IRBIT and the need to expose the GXXXP motif. In addition the apparent affinity of NBCe2-C for inhibition by Cl^-_{in} was lower than that for NBCe1-B. A more complex regulation was observed with NBCe1-A. In the basal state NBCe1-A is resistant to inhibition by physiological levels of Cl^-_{in} and is slightly stimulated by very high Cl^-_{in}. The Cl^-_{in} sensing NBCe1-A GXXXP motif seems to be a cryptic site, and deletion of part of the N terminus was required to observe the inhibition by Cl^-_{in}. This raises the possibility that the N terminus of NBCe1-A functions as a regulatory domain, similar to the N terminus of NBCe1-B, interacting with an unknown cellular factor(s). The cellular mechanism(s) that modulates the function of the NBCe1-A N terminus remains to be identified.

Regulation of NBCe1-B transport function by Cl^-_{in} is quite complex. Inhibition by the high affinity Cl^-_{in} site 1 is cryptic and is not observed until NBCe1-B is activated by IRBIT (Fig. 1), which prevents its autoinhibition (21, 23). Mutations in the first GXXXP motif prevented inhibition by Cl^-_{in} between 5 and 20 mM, whereas mutation of the second GXXXP motif in the IRBIT-activated conformation (Fig. 3*B*), combined mutations of the first and second GXXXP motifs, or deletion of the first GXXXP motif in combination with mutation of the second GXXXP motif was required to eliminate inhibition by a higher Cl^-_{in} (Fig. 3*D*). These findings suggest that NBCe1-B can sense a broad range of changes in Cl^-_{in}. In the resting state Cl^-_{in} can be as high as 60 mM (45). Under these conditions the unactivated NBCe1-B operates at approximately 40% of maximal activity, and reduction in Cl^-_{in} only gradually and modestly increases its activity. When the cells are stimulated with any IP_3-generating receptor, IRBIT is released from the IP_3 receptors (25, 27) and activates NBCe1-B (27). This likely happens while Cl^-_{in} is still high and the activity of NBCe1-B remains unchanged. Accordingly, we predict that only when Cl^-_{in} is reduced to below 20 mM the activity of NBCe1-B starts to increase and continues to do so as Cl^-_{in} continues to decline.

The complex regulation of IRBIT-activated NBCe1-B by Cl^-_{in} can potentially have several functional roles. A dramatic increase in NBCe1-B transport when Cl^-_{in} is reduced would be predicted to activate the Na^+/K^+ pump (via Na^+ influx) and cellular Cl^-/HCO_3^- exchangers (via HCO_3^- influx), thereby dampening NBCe1-B transport, increasing Cl^-_{in} and decreasing cellular ATP utilization. Hence, changes in Cl^-_{in} can serve to adjust metabolic activity. A second advantage for this mode of regulation is that the activities of NBCe1-B and the Cl^-/HCO_3^- exchangers would become reciprocally coupled in a feedback mechanism through Cl^-_{in}. For example, an increase in Cl^-/HCO_3^- exchanger activity would increase Cl^-_{in} resulting in the inhibition of NBCe1-B activity. Inhibition of NBCe1-B activity would reduce intracellular HCO_3^-, leading to a decrease in Cl^-/HCO_3^- exchanger activity and a decrease in Cl^-_{in} that would then stimulate NBCe1-B activity.

The regulation of NBCe1-B by Cl^-_{in} should have profound role in Cl^- absorbing and HCO_3^- secreting CFTR-expressing epithelia, found in the salivary and pancreatic ducts, the intestine, and the lung (7). As ductal Cl^- absorption and HCO_3^- secretion progresses, ductal Cl^-_{in} is reduced from approximately 30 to 4–5 mM (7). In the proximal portion of the duct most Cl^- exits the cells through CFTR to support HCO_3^- secretion, and in the terminal portion of the duct CFTR sets Cl^- at the low concentration of 4–5 mM as modeled in refs. 46 and 47. In

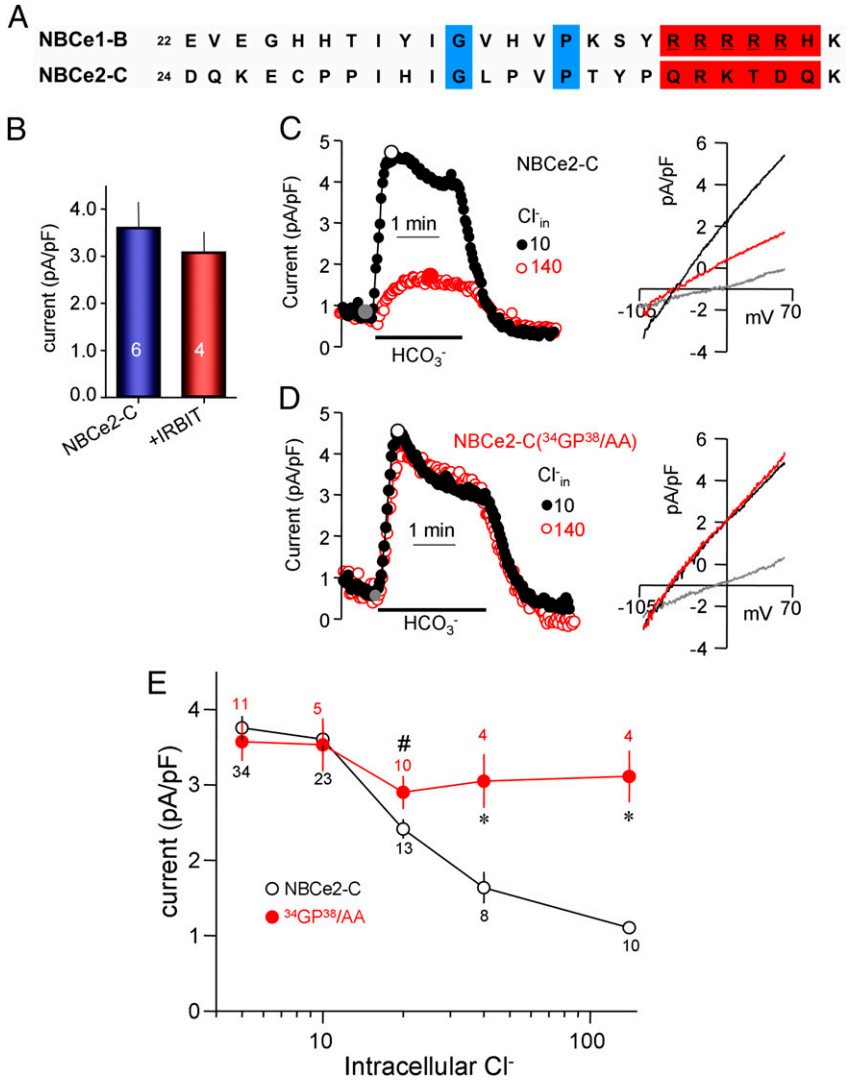

Fig. 5. A GXXXP motif-dependent regulation of NBCe2-C by Cl^-_{in}. (*A*) Position of the GXXXP motif (blue) in NBCe1-B and NBCe2-C, and lack of the arginines in NBCe2-C mediating regulation of NBCe1-B by IRBIT (red). (*B*) Lack of activation of NBCe2-C by IRBIT. (*C* and *D*) Example traces of the currents time course in pA/pF (circles) and example I/V plots for NBCe2-C (C) and NBCe2-C(^{34}GP^{38}/AA) (*D*) at 10 (black) and 140 mM Cl^-_{in} (red). (*E*) Effect of Cl^-_{in} on the activity of NBCe2-C and NBCe2-C(^{34}GP^{38}/AA). The results are plotted as mean ± SEM of the number of experiments shown next to the symbols. $^{\#}P < 0.05$, $^{*}P < 0.01$ relative to NBCe2-C.

salivary and pancreatic ducts (and likely other epithelia), fluid and electrolyte secretion is synergistically activated by Ca^{2+} and cAMP signaling pathways (27, 48, 49) that is mediated by IRBIT (27). As Cl^- is absorbed and HCO_3^- is secreted across the apical membrane by the combined actions of CFTR and SLC26a6, the luminal HCO_3^- concentration is elevated and the HCO_3^- gradient across the luminal membrane is increased. To continue transcellular HCO_3^- secretion, basolateral NBCe1-B–mediated HCO_3^- influx increases, reducing the cell-to-lumen HCO_3^- gradient and favoring continued HCO_3^- secretion. The coupling of basolateral NBCe1-B transport and apical Cl^-/HCO_3^- exchange becomes particularly crucial in the distal port of the duct where the luminal Cl^- concentration is low and the luminal HCO_3^- concentration is very high. To increase luminal HCO_3^- from approximately 120 to 140 mM requires massive HCO_3^- influx. Reduction of ductal Cl^-_{in} to 4–5 mM (19), coupled with IRBIT interaction with NBCe1-B, profoundly activates NBCe1-B to increase HCO_3^- influx and support high rate of HCO_3^- secretion.

In the present studies we focused on the modulation of NBCs by Cl^-_{in}. Sequence analysis of several additional transporters, including the Cl^- transporters, CFTR, NKCC1, NKCC2, KCC, NCC, and many SLC26 transporters, revealed that they possess at least one GXXXP motif predicted to be in a cytoplasmic domain. It will be of particular interest to determine whether the GXXXP motif(s) functions as a Cl^-_{in} sensor in other transporters.

Methods

Plasmid Construction and Solutions. The p3xFLAG-CMV-7.1/IRBIT, pEGFP-C1/NBCe1-B, pCDNA 3.1+/NBCe1-A, and pEGFP-C1/NBCe2-C constructs were described previously (23, 24, 40). The GXXXP motif mutants and deletions in NBCe1-B and NBCe1-A were generated by PCR. All constructs were verified by sequencing of the entire ORFs. In most experiments the bath solution contained 140 mM NaCl, 5 mM KCl, 1 mM $MgCl_2$, 1 mM $CaCl_2$, 10 mM Hepes (pH 7.4 with NaOH), and 10 mM glucose. Na^+-free solutions were prepared by replacing Na^+ with *N*-methyl-D-glucamine (NMDG) and Cl^--free solutions were prepared by replacing Cl^- with gluconate. HCO_3^--buffered solutions were prepared by replacing 25 mM Na^+ anion with 25 mM Na^+-HCO_3^- and reducing Hepes to 2.5 mM. HCO_3^--buffered solutions were gassed with 5% CO_2 and 95% O_2. The osmolarity of all solutions was adjusted to 310 mOsmol with the major salt.

Surface Expression and Coimmunoprecipitation. Surface expression was assayed by biotinylation of surface proteins. Cells were incubated with 0.5 mg/mL EZ-LINK Sulfo-NHS-LC-biotin (Thermo Scientific) for 30 min at 0 °C. The cells were then treated with 100 mM glycine for 10 min to terminate the biotinylation reaction, washed with PBS, and lysed with titon-based lysis buffer described previously (24). Biotinylated proteins were captured with avidin beads by incubation for 2 h at room temperature, and the precipitated proteins were analyzed by SDS/PAGE.

Coimmunoprecipitation was by incubation of extracted proteins with anti-Flag (IRBIT) and anti-α-actin (Sigma-Aldrich), and anti-GFP (NBCe1-B and NBCe2-C) (Invitrogen), antibodies with G Sepharose beads for 2 h at 0 °C. Beads were collected by brief centrifugation, washed three times with lysis buffer, and proteins were subjected to SDS/PAGE and the blots probed for the indicated proteins.

Current Measurement in HeLa Cells. The effect of Cl^-_{in} on current mediated by NBCe1-B, NBCe1-A, and NBCe2-C activity was analyzed in transiently transfected HeLa cells using whole-cell current recording at room temperature, exactly as detailed previously (24), except for varying pipette solution Cl^- between 5 and 140 mM. Patch clamp pipettes had a resistance of 5–7 MΩ when filled with KCl-based pipette solution, which allow equilibration of cytoplasmic and pipette ion composition within 20–30 s of establishing the whole-cell configuration. The cell capacitance was between 15 and 35 pF. The pipette solutions contained (in mM): 2 $MgSO_4$, 1 ATP, 0.5 EGTA, and 10 Hepes (adjusted to pH 7.3 with CsOH) and a mixture of CsCl and Cs-gluconate to yield Cl^- concentrations of 5, 10, 20, 30, 40, and 140 mM. pH was adjusted to 7.3 with CsOH. In some experiments the pipette solution contained 5 mM CsCl, 5 mM NMDG-NO_3^-, NMDG-Br^-, or NMDG-I^- and 135 mM Cs-gluconate. The Hepes-buffered bath solution contained (in mM): 140 NaCl, 5 KCl, 1 $MgCl_2$, 1 $CaCl_2$, 10 glucose, and 10 Hepes (pH 7.4 with NaOH), and the HCO_3^--buffered solution was prepared by replacing 25 mM NaCl with equimolar amount of $NaHCO_3$, and the solution was equilibrated with 5% CO_2/95% O_2. Cl^--free solutions were prepared by replacing Cl^- with gluconate. The current was recorded by 400-ms rapid alteration of membrane potential (RAMPs) from −60 to +60 mV every 2 s from a holding potential of 0 mV. Before current recording the junction potential at each pipetted solution Cl^- concentration was offset to 0 using the Axopatch 200B amplifier. The current recorded at +60 mV was used to calculate current density as pA/pF. Axopatch 200B patch-clamp amplifier, Digidata -1440A, and pClamp 10 software (Molecular Devices) were used for data acquisition and analysis. The currents were filtered at 1 kHz and sampled at 10 kHz.

Statistics. Results are given as mean ± SEM, and significance was analyzed by Student *t* test or by ANOVA.

Structure Prediction and Protein Modeling. A segment of mouse NBCe1-B, consisting of 1,000 amino acids (National Center for Biotechnology Information reference sequence NP_061230.2), was submitted to both ROBETTA (50) and HHPred servers (Max Planck Institute of Developmental Biology). In general, both servers provided roughly similar homology templates. We selected one of five coordinates generated by ROBETTA in which the AID was linked to the homologous domain with a hinge that might allow rotation during activation by IRBIT. One domain spanning residues 1–100 was identified to be homologous to the Yeast Mitochondrial Processing Peptidase (Protein Data Bank ID 1hr6), another region encompassing residues 101–430 is homologous to human erythrocyte band 3 cytoplasmic domain (Protein Data Bank ID 1HYN) as we previously reported (24). The transmembrane segment spanning residues 431–1000 was identified to be homologous to the crystal structure of the Uracil Transporter UraA (Protein Data Bank ID 3qe7). The coordinates provided by the ROBETTA server were used to generate the final model with PyMOL software.

ACKNOWLEDGMENTS. This work was funded in part by Intramural Research Program of the NIH, National Institute of Dental and Craniofacial Research Grant Z1A-DE000735 (to S.M.), by fellowships from the Nakatomi, Sumitomo Life Welfare and Culture and the Mochida Memorial Foundations (O.Y.), by the National Research Foundation of Korea grant funded by the Korea government [Ministry of Science, ICT and Future Planning (MSIP)] (2012R1A2A1A01003487) (to D.M.S.), and by NIH Grant R01-DK077162, the Allan Smidt Charitable Fund, the Factor Family Foundation, and the Arvey Foundation (I.K.).

1. Gagnon KB, Delpire E (2012) Molecular physiology of SPAK and OSR1: Two Ste20-related protein kinases regulating ion transport. *Physiol Rev* 92(4):1577–1617.
2. Romero MF, Chen AP, Parker MD, Boron WF (2013) The SLC4 family of bicarbonate (HCO_3^-) transporters. *Mol Aspects Med* 34(2-3):159–182.
3. Ohana E, Yang D, Shcheynikov N, Muallem S (2009) Diverse transport modes by the solute carrier 26 family of anion transporters. *J Physiol* 587(Pt 10):2179–2185.
4. Parker MD, Boron WF (2013) The divergence, actions, roles, and relatives of sodium-coupled bicarbonate transporters. *Physiol Rev* 93(2):803–959.
5. Stauber T, Weinert S, Jentsch TJ (2012) Cell biology and physiology of CLC chloride channels and transporters. *Compr Physiol* 2(3):1701–1744.
6. Kunzelmann K, et al. (2011) Anoctamins. *Pflugers Arch* 462(2):195–208.
7. Lee MG, Ohana E, Park HW, Yang D, Muallem S (2012) Molecular mechanism of pancreatic and salivary gland fluid and HCO3 secretion. *Physiol Rev* 92(1):39–74.
8. Yu H, Zhang Z, Lis A, Penner R, Fleig A (2013) TRPM7 is regulated by halides through its kinase domain. *Cell Mol Life Sci* 70(15):2757–2771.
9. Plested AJ (2011) Kainate receptor modulation by sodium and chloride. *Adv Exp Med Biol* 717:93–113.
10. Chaudhry C, Plested AJ, Schuck P, Mayer ML (2009) Energetics of glutamate receptor ligand binding domain dimer assembly are modulated by allosteric ions. *Proc Natl Acad Sci USA* 106(30):12329–12334.
11. Succol F, Fiumelli H, Benfenati F, Cancedda L, Barberis A (2012) Intracellular chloride concentration influences the GABAA receptor subunit composition. *Nat Commun* 3:738.
12. Menegazzi R, Busetto S, Cramer R, Dri P, Patriarca P (2000) Role of intracellular chloride in the reversible activation of neutrophil beta 2 integrins: A lesson from TNF stimulation. *J Immunol* 165(8):4606–4614.
13. Blackiston DJ, McLaughlin KA, Levin M (2009) Bioelectric controls of cell proliferation: Ion channels, membrane voltage and the cell cycle. *Cell Cycle* 8(21):3527–3536.
14. Tresguerres M, Levin LR, Buck J (2011) Intracellular cAMP signaling by soluble adenylyl cyclase. *Kidney Int* 79(12):1277–1288.
15. Ko SB, et al. (2004) Gating of CFTR by the STAS domain of SLC26 transporters. *Nat Cell Biol* 6(4):343–350.
16. Boron WF, Chen L, Parker MD (2009) Modular structure of sodium-coupled bicarbonate transporters. *J Exp Biol* 212(Pt 11):1697–1706.
17. Kurtz I (2013) SLC4 sodium-driven bicarbonate transporters. *Seldin and Giebisch's The Kidney: Physiology and Pathophysiology*, eds Alperin RJ, Caplan M, Moe OW (Elsevier/Academic, Amsterdam), pp 1837–1860.
18. Song Y, et al. (2012) Deletion of Slc26a6 alters the stoichiometry of apical Cl-/HCO-3 exchange in mouse pancreatic duct. *Am J Physiol Cell Physiol* 303(8):C815–C824.
19. Ishiguro H, et al. (2002) Chloride transport in microperfused interlobular ducts isolated from guinea-pig pancreas. *J Physiol* 539(Pt 1):175–189.
20. Kao L, et al. (2011) Severe neurologic impairment in mice with targeted disruption of the electrogenic sodium bicarbonate cotransporter NBCe2 (Slc4a5 gene). *J Biol Chem* 286(37):32563–32574.
21. Shirakabe K, et al. (2006) IRBIT, an inositol 1,4,5-trisphosphate receptor-binding protein, specifically binds to and activates pancreas-type Na+/HCO3- cotransporter 1 (pNBC1). *Proc Natl Acad Sci USA* 103(25):9542–9547.
22. Yang D, et al. (2011) IRBIT governs epithelial secretion in mice by antagonizing the WNK/SPAK kinase pathway. *J Clin Invest* 121(3):956–965.
23. Yang D, et al. (2009) IRBIT coordinates epithelial fluid and HCO3- secretion by stimulating the transporters pNBC1 and CFTR in the murine pancreatic duct. *J Clin Invest* 119(1):193–202.
24. Hong JH, et al. (2013) Convergence of IRBIT, phosphatidylinositol (4,5) bisphosphate, and WNK/SPAK kinases in regulation of the Na+-HCO3- cotransporters family. *Proc Natl Acad Sci USA* 110(10):4105–4110.
25. Ando H, et al. (2006) IRBIT suppresses IP3 receptor activity by competing with IP3 for the common binding site on the IP3 receptor. *Mol Cell* 22(6):795–806.
26. Ando H, Mizutani A, Matsu-ura T, Mikoshiba K (2003) IRBIT, a novel inositol 1,4,5-trisphosphate (IP3) receptor-binding protein, is released from the IP3 receptor upon IP3 binding to the receptor. *J Biol Chem* 278(12):10602–10612.
27. Park S, et al. (2013) Irbit mediates synergy between ca(2+) and cAMP signaling pathways during epithelial transport in mice. *Gastroenterology* 145(1):232–241.
28. Dinudom A, Young JA, Cook DI (1993) Na+ and Cl- conductances are controlled by cytosolic Cl- concentration in the intralobular duct cells of mouse mandibular glands. *J Membr Biol* 135(3):289–295.
29. Park HW, et al. (2010) Dynamic regulation of CFTR bicarbonate permeability by [Cl-]i and its role in pancreatic bicarbonate secretion. *Gastroenterology* 139(2):620–631.
30. Aharonovitz O, et al. (2001) Modulation of Na+/H+ exchange activity by Cl-. *Am J Physiol Cell Physiol* 281(1):C133–C141.
31. Robertson MA, Foskett JK (1994) Na+ transport pathways in secretory acinar cells: Membrane cross talk mediated by [Cl-]i. *Am J Physiol* 267(1 Pt 1):C146–C156.
32. Dutzler R, Campbell EB, Cadene M, Chait BT, MacKinnon R (2002) X-ray structure of a ClC chloride channel at 3.0 A reveals the molecular basis of anion selectivity. *Nature* 415(6869):287–294.
33. Faraldo-Gómez JD, Roux B (2004) Electrostatics of ion stabilization in a ClC chloride channel homologue from *Escherichia coli*. *J Mol Biol* 339(4):981–1000.
34. Bergsdorf EY, Zdebik AA, Jentsch TJ (2009) Residues important for nitrate/proton coupling in plant and mammalian CLC transporters. *J Biol Chem* 284(17):11184–11193.
35. Zdebik AA, et al. (2008) Determinants of anion-proton coupling in mammalian endosomal CLC proteins. *J Biol Chem* 283(7):4219–4227.
36. Ohana E, Shcheynikov N, Park M, Muallem S (2012) Solute carrier family 26 member a2 (Slc26a2) protein functions as an electroneutral SOFormula/OH-/Cl- exchanger regulated by extracellular Cl-. *J Biol Chem* 287(7):5122–5132.

37. Bae JS, et al. (2013) Chaperone stress 70 protein (STCH) binds and regulates two acid/base transporters NBCe1-B and NHE1. *J Biol Chem* 288(9):6295–6305.
38. McAlear SD, Liu X, Williams JB, McNicholas-Bevensee CM, Bevensee MO (2006) Electrogenic Na/HCO3 cotransporter (NBCe1) variants expressed in *Xenopus* oocytes: Functional comparison and roles of the amino and carboxy termini. *J Gen Physiol* 127(6):639–658.
39. Virkki LV, Wilson DA, Vaughan-Jones RD, Boron WF (2002) Functional characterization of human NBC4 as an electrogenic Na+-HCO cotransporter (NBCe2). *Am J Physiol Cell Physiol* 282(6):C1278–C1289.
40. Sassani P, et al. (2002) Functional characterization of NBC4: A new electrogenic sodium-bicarbonate cotransporter. *Am J Physiol Cell Physiol* 282(2):C408–C416.
41. Glykys J, et al. (2014) Local impermeant anions establish the neuronal chloride concentration. *Science* 343(6171):670–675.
42. Yamada J, et al. (2004) Cl- uptake promoting depolarizing GABA actions in immature rat neocortical neurones is mediated by NKCC1. *J Physiol* 557(Pt 3):829–841.
43. Miyazaki H, Shiozaki A, Niisato N, Marunaka Y (2007) Physiological significance of hypotonicity-induced regulatory volume decrease: Reduction in intracellular Cl- concentration acting as an intracellular signaling. *Am J Physiol Renal Physiol* 292(5):F1411–F1417.
44. Zhao H, Muallem S (1995) Na+, K+, and Cl- transport in resting pancreatic acinar cells. *J Gen Physiol* 106(6):1225–1242.
45. Zhao H, Xu X, Diaz J, Muallem S (1995) Na+, K+, and H+/HCO3- transport in submandibular salivary ducts. Membrane localization of transporters. *J Biol Chem* 270(33):19599–19605.
46. Sohma Y, Gray MA, Imai Y, Argent BE (2001) 150 mM HCO3(-)–how does the pancreas do it? Clues from computer modelling of the duct cell. *JOP* 2(4 Suppl):198–202.
47. Yamaguchi M, et al. (2009) Apical Cl-/HCO3- exchanger stoichiometry in the modeling of HCO3- transport by pancreatic duct epithelium. *J Med Invest* 56(Suppl):325–328.
48. Lee RJ, Foskett JK (2010) cAMP-activated Ca2+ signaling is required for CFTR-mediated serous cell fluid secretion in porcine and human airways. *J Clin Invest* 120(9): 3137–3148.
49. Choi JY, et al. (2007) Synergistic airway gland mucus secretion in response to vasoactive intestinal peptide and carbachol is lost in cystic fibrosis. *J Clin Invest* 117(10): 3118–3127.
50. Kim DE, Chivian D, Baker D (2004) Protein structure prediction and analysis using the Robetta server. *Nucleic Acids Res* 32(Web Server issue):W526–W531.